Effect of post-curing process on the performance of automotive 3D-printed specimens

Forough Zareanshahraki[a], Amelia Davenport[b], Neil Cramer[b], Christopher Seubert[c], Ellen Lee[c], Matthew Cassoli[c]

a. Coatings Research Institute, Eastern Michigan University, Ypsilanti, MI

b. Colorado Photopolymer Solutions, Boulder, CO

c. Research and Innovation Center, Ford Motor Company, Dearborn, MI

Abstract

The final material properties of 3D-printed parts that utilize UV curable resins are highly dependent on any post-cure processing used after printing. This post-cure step is needed to crosslink unreacted double bonds remaining after the print process is complete. However, differences in part geometry, pigmentation, stabilization, and resin formulation can make it difficult to employ a generic, one-size-fits-all post-cure process.

In this study, the effect of the post-curing process on the mechanical properties of three different 3D-printable, non-stabilized UV-curable resin systems was studied. Two of the systems (A and B) used thiol-ene-based chemistries, while the third one (C) used acrylate-based chemistry. To this end, ASTM D638 type IV tensile bars were printed using a DLP printer and post-cured using one of five different processes: no post-cure, UV-only, heat-only, UV+ heat, and electron beam (EB) curing. Bulk tensile properties and nano-hardness values were measured for each of the systems and post-cure conditions.

Results indicated that post-cure process had a significant effect on the final performance of the resins, and was dependent on the chemistry. Thermal curing was not as effective as UV for System C compared to the two other systems, which could undergo thermal polymerization as well. System B, however, showed the smallest change in mechanical properties before and after post-curing, regardless of the type of post-curing. EB post-curing, even at very low dosages, i.e. from 0.05 Mrad to 1 Mrad, resulted in considerable crosslinking, to the point of embrittlement and a significant drop in percent elongation at break (%E) above 0.5 Mrad of dosage. Overall, provided a suitable post-curing process was employed, all the systems demonstrated promising potential for automotive applications.

Keywords: additive manufacturing, 3D-printing, automotive, post-curing, nano-indentation, digital light processing (DLP)

1. Introduction

3D-printing is an additive manufacturing (AM) process in which layers of material are successively deposited on top of each other to form a 3D object. New advances in 3D-printing have opened new horizons to more robust designs with lower costs and reduced lead times in various fields, including the automotive industry[1,2]. Technological advancements in AM have enabled the fabrication of 3D objects from a wide range of raw materials including metals, ceramics, fibers, as well as polymers, which are the focus of this study[3]. Thermoplastic polymers are usually processed by melt-type 3D-printing methods, such as fused filament fabrication (FFF) and selective laser sintering (SLS). However, these techniques usually result in relatively low resolution, and in the case of FFF, slow processing and weak interlayer adhesion. In order to

address these problems, new 3D-printing technologies, which use thermoset resins, have emerged. Vat photopolymerization is one of these techniques, which is based on selective photopolymerization of a light-reactive liquid resin in a reservoir.[4]

Photopolymerization is a widely used polymerization mechanism in many engineering applications such as coatings[5–8]and dental restoration[9], thanks to advantages such as rapid curing, low to zero VOC formulations, and low capital investment[10]. Due to chemistry-related innovations, photopolymerization-based 3D-printing techniques have attracted special attention in the past decades[4]. In addition to the aforementioned advantages, photopolymerization offers other attractive benefits in 3D-printing. Versatility and high spatial/temporal control over photopolymerization reactions can significantly enhance the printing resolution and speed in such technologies. Moreover, higher interactions between the layers lead to improved mechanical properties. Stereolithography (SLA), digital light processing (DLP), and continuous liquid interface production (CLIP) are examples of photopolymerization-based 3D-printing techniques. The main differences between these techniques are the source and pattern of radiation as well as the mechanism of separation of the printed layer from the vat.

Materials used in 3D photopolymerization printing are photosensitive liquid oligomers and monomers that can rapidly convert to a solid polymeric network upon exposure to radiation. In the most common free-radical photopolymerization process, under irradiation, the photoinitiator decomposes into active radicals, which attach to monomers to initiate the photopolymerization reaction. The activated monomers then react with carbon double bonds of unsaturated monomers, increasing the polymer chain lengths. The propagated polymer chains then start to connect to form a network structure, solidifying the liquid polymer. During this process, the material properties of the cured material change dramatically. Examples of photosensitive chemistries include acrylates and thiol-enes. The latter proceeds via a step-growth polymerization (see **Figure 1 (a)**) and is reported to offer no inhibition to oxygen, delayed gel times, more homogenous networks, and lower shrinkage stress compared to the conventional acrylate systems that polymerize through a chain-growth mechanism[11] (see **Figure 1 (b)**). These unique features make thiol-ene an ideal chemistry for DLP printing [4,12].

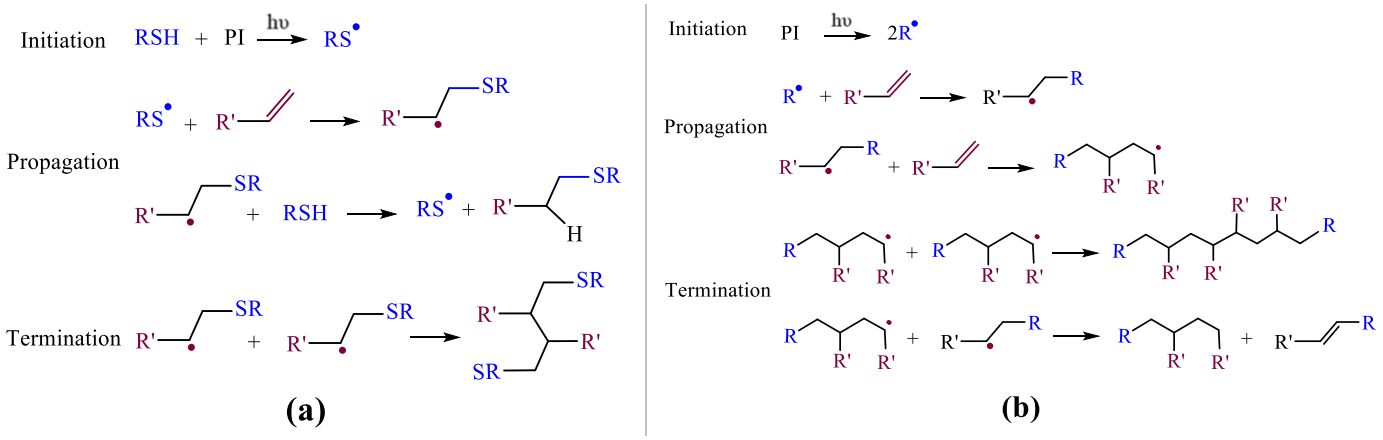

Figure 1: (a) step-growth mechanism of thiol-ene photopolymerization; (b) chain growth mechanism of acrylates photopolymerization

To ensure an acceptable z-direction resolution during printing, the penetration depth of the UV light into the resin solution is typically limited by using various UV absorbers, such as pigments or dyes. As a result, complete conversion of the carbon double bonds usually does not occur during the printing process. This post-print conversion state is referred to as the "green state". In their green state, the printed parts typically contain unreacted species that can undergo additional crosslinking when exposed to UV light. If this UV exposure occurs during service, it can change the part's mechanical properties over time, which is not desirable in the automotive industry[13].

A post-curing step is often employed after printing to crosslink some of the unreacted species before the parts are put into service. However, differences in part geometry, pigmentation, stabilization, and resin formulation can make it difficult to employ a universal, one-size-fits-all post-cure process. For instance, Zguris's studies clearly demonstrated that different 3D photopolymerizable resins require different time and temperature conditions to reach full-cure and show good chemical performance[14]. On the other hand, most of the former literature on mechanical properties of 3D-printed parts is concentrated on the effect of various processing parameters[15–19], and to the best of our knowledge, a detailed study of the effect of the post-curing process on the performance of 3D-printed automotive parts is lacking. Therefore, there is a need to delve deeper into this subject.

The purpose of this study was to investigate the effect of the post-cure process on the performance of 3D-printed materials based on acrylate and thiol-ene chemistries. The effect of the post-curing process on the mechanical properties of three different 3D-printable, UV-curable resin formulations (Systems A and B with thiol-ene chemistry, and System C with acrylate chemistry) was studied. ASTM D638 Type IV tensile bars were printed using a digital light processing (DLP) printer and post-cured using one of five different processes: no post-cure, UV-only, heat-only, UV+ heat, and electron beam (EB) curing. Bulk tensile properties and nano-hardness values were measured for each of the systems and post-cure conditions.

2. Experimental

2.1. Materials

The three UV-curable resin formulations used in this study were provided by Colorado Photopolymer Solutions (CPS) (Boulder, CO). As previously mentioned, Systems A and B were based on thiol-ene chemistry, while System C was formulated from conventional acrylates. The alkene source in System B contains a low molecular weight aromatic heterocycle structure, while System A contains high molecular weight aliphatic urethane acrylates. Therefore, System B comprises more functional groups, which makes it more reactive than System A in nature. It should be mentioned that these systems did not include any hindered amine light stabilizers (HALS) in their formulations for light stabilization. However, the formulation did contain carbon black as a strong UV-absorber to ensure a good z-resolution.

2.2. Methods

2.2.1. Printing method

A series of type IV dumbbell-shape tensile bars, with dimensions as described in ASTM D638, were printed with an Origin One DLP printer, using the printing parameters as described in the CPS technical datasheets, and a 75µm layer thickness. The bottom surface of the resin vat in this printer is composed of a transparent polytetrafluoroethylene (PTFE) sheet to facilitate detachment

of the printed layer from the vat. The UV source in the printer emits light at a wavelength of 385 nm with an intensity of 5 mW/m^2. The area of UV light illumination is 144 mm × 81 mm.

The 3D-printing process occurred as follows: First, the geometry of the sample was modeled using a computer aided design (CAD) program. Next, this model was converted to an image of slices, i.e., a series of thin layers that together form the whole sample. Afterward, the motor-powered build platform was moved down until the gap between the PTFE sheet and the platform was equal to the intended layer thickness (75µm in this study). The image of the layer was then projected through the vat bottom onto the build platform, using UV light for a specific time period (25 s exposure for the 1st layer, 10 s exposure for layers 2-6, and 3 s exposure for all the next layers). Finally, the UV light was turned off, and the platform moved up so that the photopolymer resin could flow back to the projected area. The former steps were repeated until the sample was completely printed[20,21]. After being printed, the samples were placed in an ultrasonicated IPA bath for 3 minutes to clean off any uncured resin, followed by drying in an oven at 25°C (**Fig. 2**). All the samples were then wrapped in aluminum foil and kept in a dark place to prevent any additional light-induced polymerization before testing.

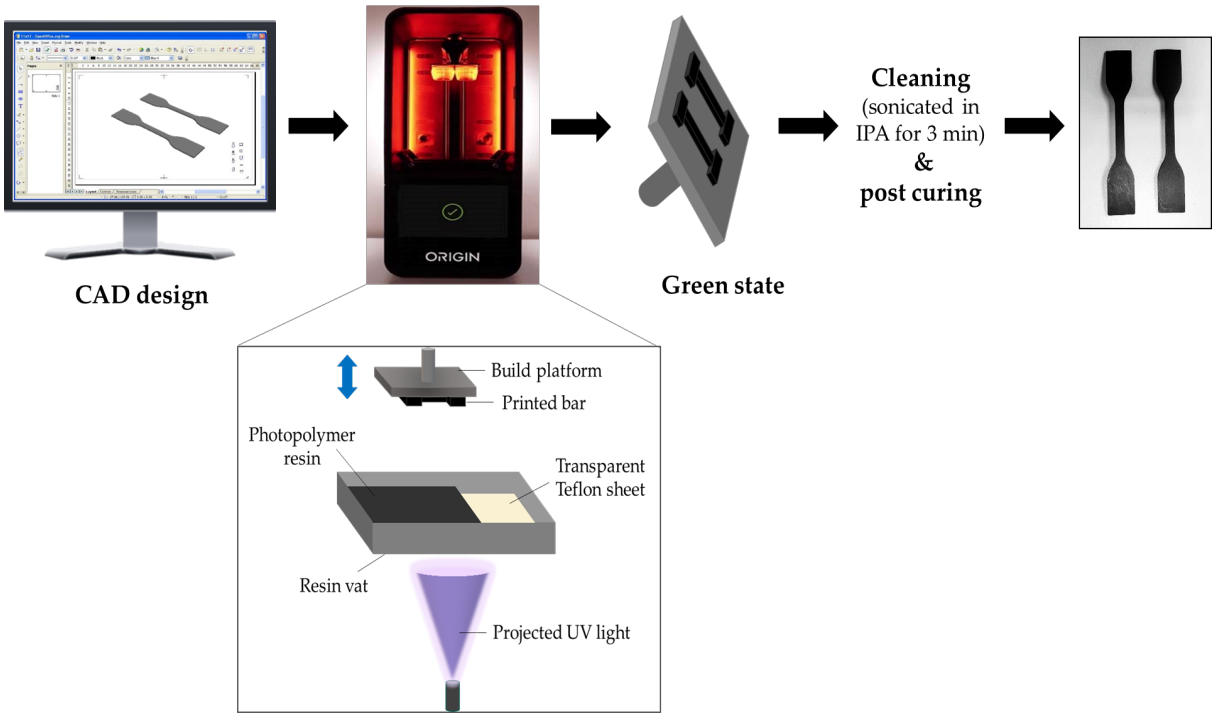

Figure 2: Schematic set-up of a DLP 3D-printer

2.2.2. Post-curing process

The printed samples were post-cured using one of the following processes: no post-cure, UV-only, heat-only, and UV+heat. As a complementary study, the effect of EB-curing was also studied for System B only, which demonstrated the most desirable mechanical properties among all the systems. Thermal post-curing was conducted by placing the samples in an oven for 1h at 150 °C. An ELC-4001 UV Flood system, with a broad spectrum lamp was used for UV post-curing. UV-curing was performed for four minutes and thirty seconds on each side of the samples, i.e., a

total curing time of nine minutes. EB-curing of the samples were post-cured by EB irradiation film using an EB accelerator equipped with a variable speed, fiberglass carrier web (Broad Beam EP Series, PCT E-beam and Integration, LLC, Davenport, IA, USA).

2.2.3. Tensile properties

The tensile properties of the specimens were measured by an Instron 3366 tensile machine, using a 30-kN load cell, 65 mm initial distance between the grips, and a 25-mm extensometer according to ASTM D638. Five test specimens were tested and averaged for each post-cure condition. The testing was carried out at a constant displacement rate of 5 mm/min in ambient conditions.

2.2.4. Nano-hardness

In order to study the nano-harness profile in various depths, a strip of each sample, which had been cut using a manual cutter, was cold-mounted in epoxy resin and polished. Polishing was conducted in an order of 600, 1200, and 2400 grit #, followed by fine polishing using abrasive slurries, in an order of 5 µm, 3 µm, 1 µm, and 0.3 µm. An Anton Paar (Graz, Austria) nano-indentation Tester (NHT^3) was used to measure the nano-hardness of the samples. The major components of this instrument include a mobile indenter head, an optical microscope attached to a video camera, and a sample holder rigidly fixed to an x–y–z motorized table. The Berkovich indenter, mounted on the indenter head, is a three-sided triangular-based pyramidal diamond with a well-defined geometry, capable of making well-defined indentation impressions, as shown in **Figure 3 (a)**.

During the nano-indentation process, the Berkovich tip approaches the surface of the sample. The force-displacement data is used to determine the point of contact. After the sample is contacted, the force is linearly increased, and the tip indents into the surface of the sample. A short dwell time occurs at the maximum load, 50 mN in this case, and then the sample is unloaded. At the initial point of unloading, the hardness (H) is measured. In this study, Oliver and Phaar's method[22] was used to calculate the hardness by dividing the maximum load, P_{max}, by the contact area of indent (A), as described in equation 1. The indents were made along a path of 50 µm in the x-direction and 50 µm in the y-direction, to a total length of approximately 350 µm (**Figure 3 (b)**). Eight different indentations were used to calculate the average hardness as a function of depth.

$$H = \frac{P_{max}}{A} \qquad (1)$$

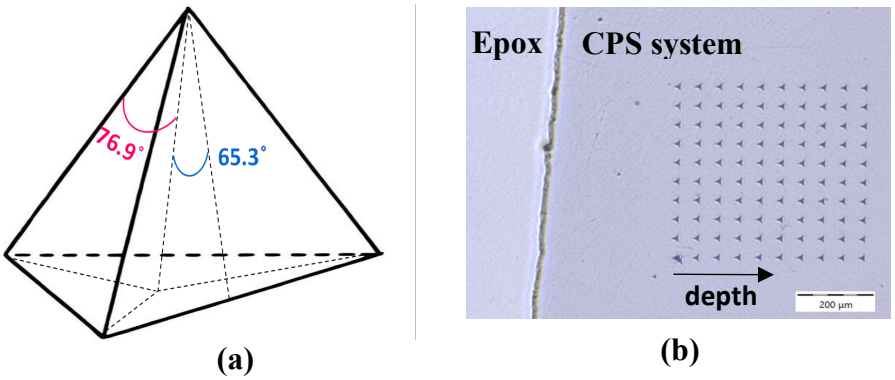

(a) **(b)**

Figure 3: (a) typical shape of indentation by Berkovich tip; (b) Microscopic image of indents in this study

2.2.5. Fourier-transform infrared (FTIR) spectroscopy

Fourier-transform infrared (FTIR) spectra were collected to study the nature of reactions induced by heat and EB curing in the thiol-ene systems. Spectra were measured using KBr standard disks on Bruker Tensor 27 FTIR analyzer at 64 scans and 2 cm^{-1} of resolution in the frequency range of 400–4000 cm^{-1} .

3. Results and Discussions

3.1. Effect of post-curing process on the tensile properties

The effects of the post-curing method on the tensile strength, Young's modulus, and percent elongation at break (%E) were studied for Systems A, B, and C.

For System A, regardless of the post-curing method, tensile strength and Young's modulus both improved during post-cure, as demonstrated in **Figure 4**. Tensile strength increased by ~200%, from 11.2 MPa to 33.7 MPa, and Young's modulus increased by 111%, from 758 MPa to ~1600 MPa. However, %E reduced by more than 85%, from 27.3 to ~3.5. Both the UV and thermal post-cure steps produced similar tensile properties because thiol-ene systems can undergo polymerization via radiation[11] or heating[23] processes. The significant reduction in %E after post-curing might not be ideal in automotive parts that require a high amount of %E retention during their service life. System A might be a good option for parts that need high flexibility, but are not exposed to mechanical forces that can induce dimensional changes, such as decorative parts or badges.

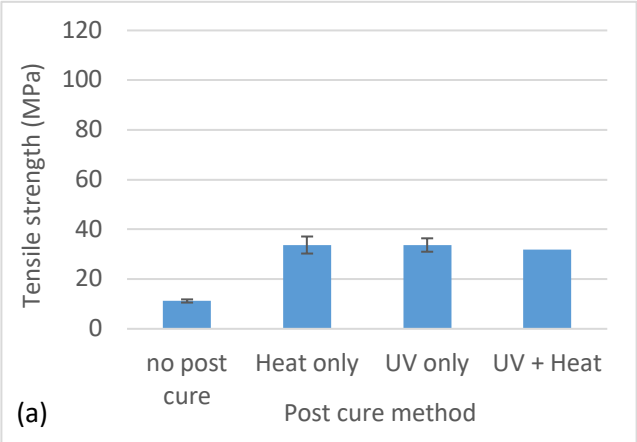

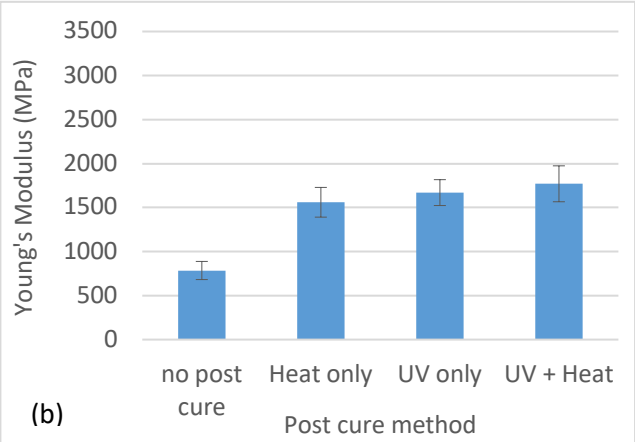

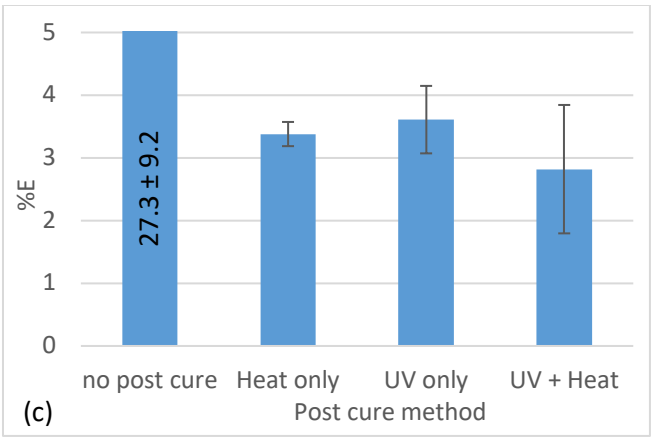

Figure 4: Effect of post-curing process on tensile properties of System A: (a) Tensile strength; (b) Young's modulus; (c) %E

For System C, an acrylate based system, thermal post-curing was not as effective as UV-post-curing (as shown in **Figure 5**). According to the results, UV-curing resulted in ~285% increase in tensile strength, from 21 MPa to 104 MPa, and 274% increase in Young's modulus, from 1174 MPa to 4390 MPa., while these values were about ~45% (from 27.1 MPa to 39.5 MPa) and ~109.6% (from 1174 MPa to 2461 MPa) for heat post-curing, respectively. While it is known that acrylate groups can undergo thermal polymerization [24], this system did not contain any thermal initiators, so it is unlikely any significant crosslinking occurred as a result of the 150°C/ 1 hour "heat only" post-cure step. As a result, UV post-curing seems to provide the best tensile properties among all post-curing processes for System C. However, System C exhibited a similar post-cure reduction in %E to that of System A, e.g., UV post-curing decreased %E by 58%, from 7.9 to 3.3. This again means System C should not be used in applications that may significantly stress or load the part. Utilization of both UV and thermal post-curing together had a negative effect on mechanical properties of this system for unknown reasons. Some possible reasons could be rapid degradation of the UV-cured sample after being heated at 150°C for one hour.

Finally, for System B, post-curing did not have a considerable effect on the tensile properties, as depicted in **Figure 6**. Post-curing processes improved the tensile strength and Young's modulus slightly, and did not result in significant reduction of %E as was the case with the two other systems. While systems A and B are both thiol-ene systems, System B includes a heterocyclic core structure with lower molecular weight, and in turn, higher functionalities than System A. Thus, these systems show a different behavior upon post-curing. The UV radiation during the printing process likely resulted in a vitrified network with limited segmental mobility that hindered further conversion of unreacted groups. This vitrification effect was slightly mitigated by heat treatment in case of UV + Heat post-curing. Moreover, higher functionalities can mitigate the oxygen inhibition effect more effectively, which, in turn, can result in higher conversions. According to the results, it seems that ample crosslinking of the free radicals occurs during the printing process. Therefore, post-curing does not seem to be necessary for System B, which could be beneficial in high volume manufacturing environments. Considering the aforementioned points, System B could be a promising option for the automotive parts that require good retention of tensile properties, including %E.

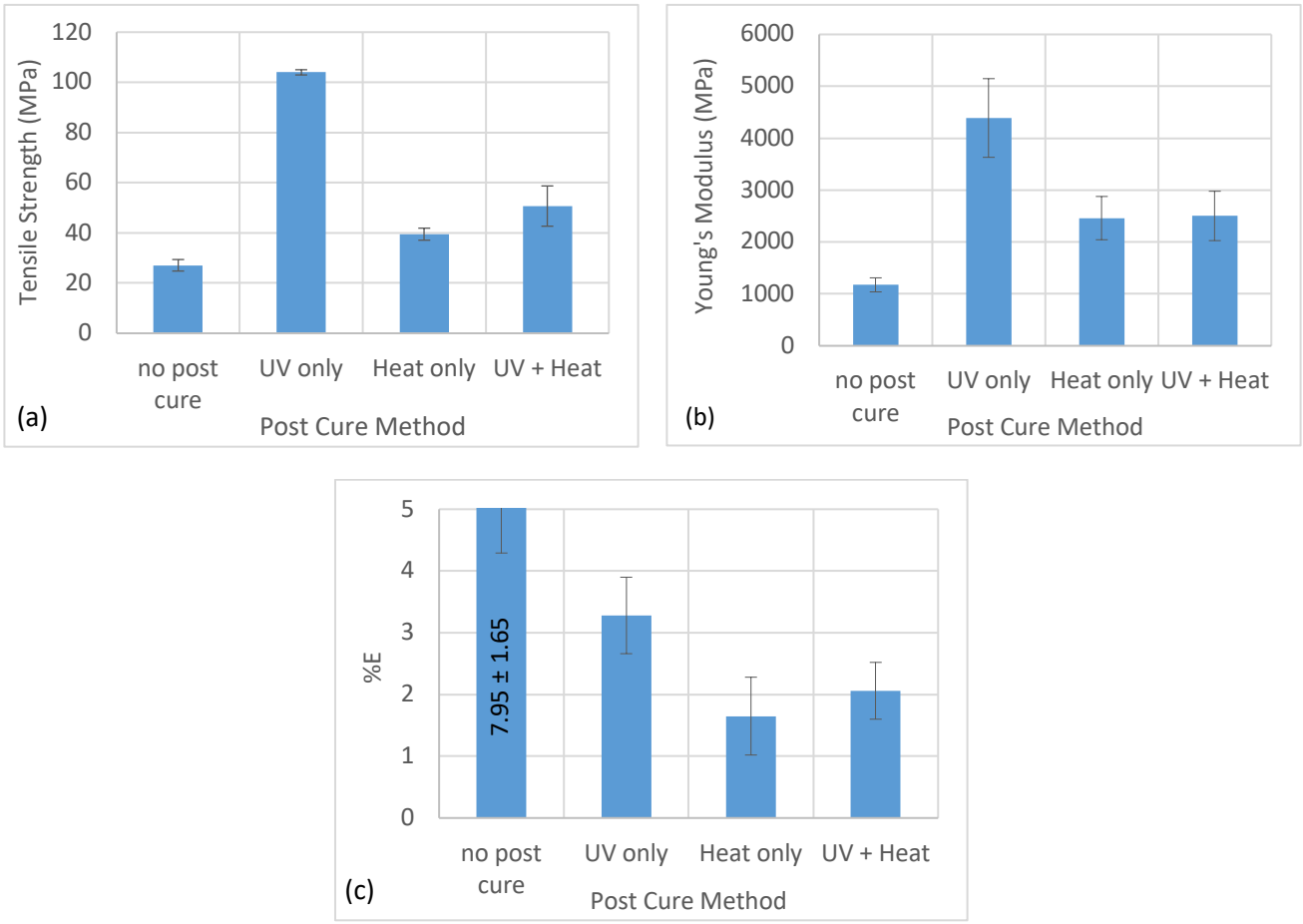

Figure 5: Effect of post-curing process on tensile properties of System C:
(a) Tensile strength; (b) Young's modulus; (c) %E

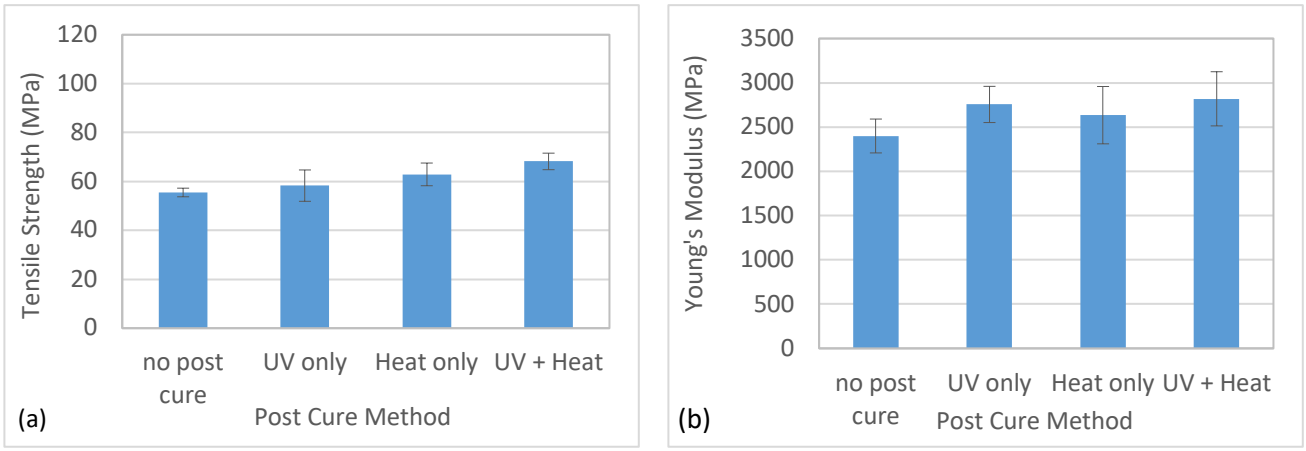

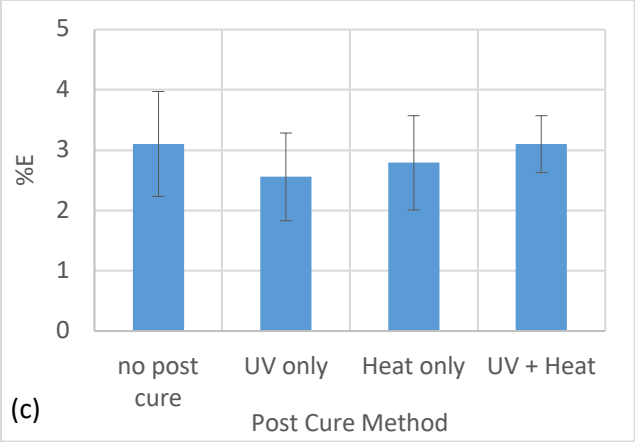

Figure 6: Effect of post-curing process on tensile properties of System B: (a) Tensile strength; (b) Young's modulus; (c) %E

To assess the effectiveness of an electron beam (EB) post-cure process, System B samples were exposed to varying levels of EB radiation. EB-curing through free radical polymerization differs from UV-curing mainly in the initiation process. No photoinitiator is needed in the EB process because the energy of EB is high enough to form the initiative species by cleavage of a bond located on the monomer[25]. Since the initiating radical is formed from the resin itself, rather than from an added initiator, EB-curing allows for a small amount of additional crosslinking compared to UV-curing[26]. EB-cure systems are known to have the draw-back of being inhibited by oxygen, and therefore, EB-curing is usually conducted in an inert atmosphere, like nitrogen. However, this drawback could be overcome by the utilization of thiol-ene chemistry. All these advantages make the EB-curable thiol-ene resin systems an interesting option for DLP 3D-printing.

As shown in **Figure 7**, higher dosages of EB post-cure (i.e., one-step 5, 10, and 20 Mrad) resulted in significant embrittlement of samples of System B compared to standard UV post-curing. %E values were reduced by ~ 50%, regardless of the dosage. Moreover, increasing the EB dosage from 5 to 20 Mrad decreased the tensile strength by ~38%, from 50.6 to 31.2 MPa, while increased the Young's modulus by ~ 27%, from 2732 to 3480. It was unknown if this was simply due to an excess of EB dosage or if the samples were heated during the EB post-curing process. Therefore, two changes were made to the EB post-curing process. First, EB-curing was conducted in successive 2.5 Mrad steps for dosages greater than 2.5 Mrad, with a pause between successive exposures to cool the samples in ambient conditions in order to eliminate the effect of heat-curing as much as possible (**Figure 7**). Although step-by-step curing in higher dosages improved tensile strength and Young's modulus to some extent, %E was still far from the values achieved using the standard UV post-cure method. Second, EB post-curing dosages were reduced to: 0.05, 0.1, 0.5, 1 and 2.5 Mrad (**Figure 8**). Reducing EB dosages resulted in higher %E values. Dosages less than 2.5 Mrad resulted in Young's modulus values close to that of standard UV post-cure, and tensile strengths more than that of UV post-cure. These results indicate that higher dosages of EB likely induce excessive crosslinking of the system, which will be investigated in our future studies using Raman spectroscopy.

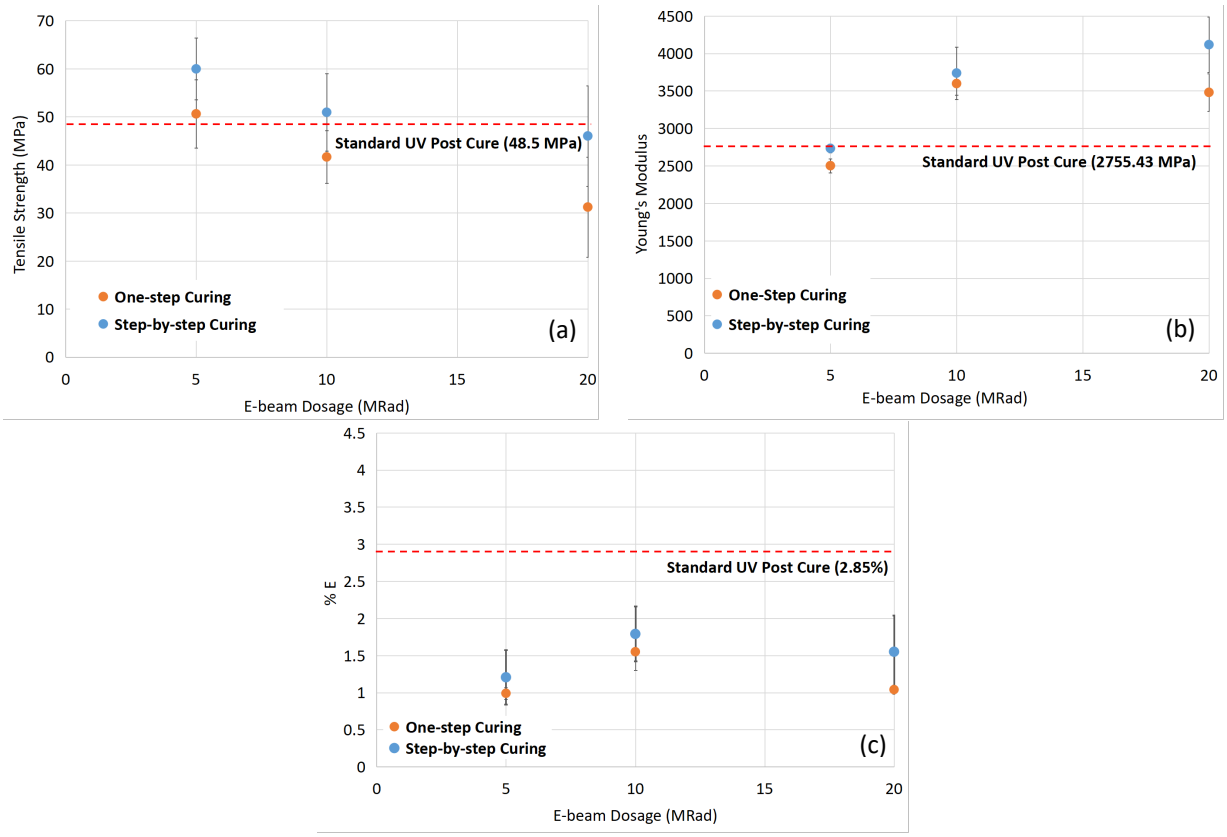

Figure 7: Effect of one-step versus step-by-step EB post-curing on tensile properties of System B: (a) Tensile strength; (b) Young's modulus; (c) %E

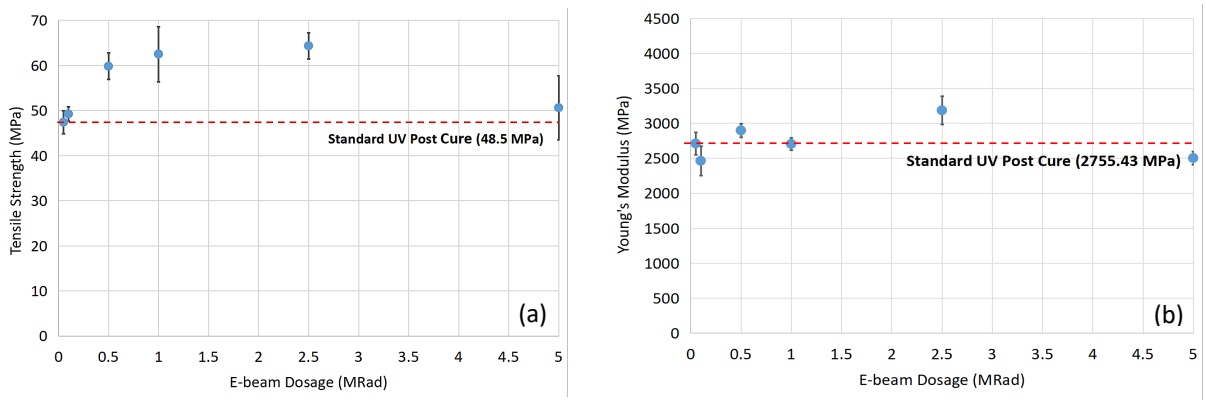

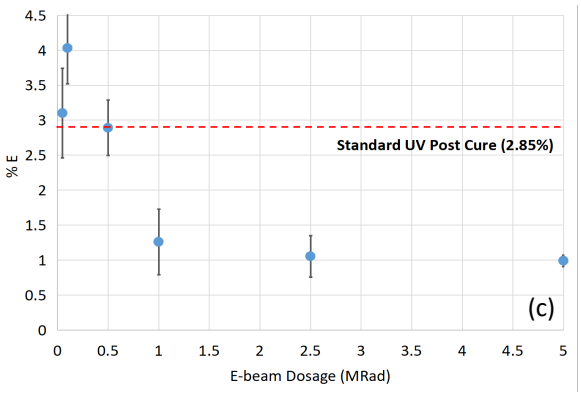

Figure 8: Effect of EB post-curing with low dosages on tensile properties of System B: (a) Tensile strength; (b) Young's modulus; (c) %E
(b)

3.2. Effect of post-curing process on nano-hardness

To study the nano-hardness profile, as an approximation of the cure state at various depths, a strip of each sample was cold-mounted in epoxy resin to be polished. Depth profiling was conducted in order to assess any possible gradient in cure state exists for different post-curing methods. **Figure 9** shows that the surface nano-hardness of System C increased by more than 200% after post-curing (from ~50 to >150 MPa) regardless of the process used. Moreover, no gradient in hardness as a function of depth was observed, which is particularly interesting in the case of UV-curing. Heat-curing showed a similar trend.

For System B, nano-hardness results were in good agreement with the tensile properties, i.e., the nano-hardness was slightly improved, regardless of the post-curing process (see **Figure 10**). Similarly, nano-hardness was observed to be independent of depth, showing a uniform conversion as a function of depth.

When cured by UV-only, System A showed a gradient in hardness as a function of depth, i.e., the hardness decreased as the depth increased. This might be due to the higher UV absorption of this system, which limits the depth of cure. However, further research, e.g. Raman microscopy and UV-Vis spectroscopy studies, are needed to effectively investigate the possible reasons.

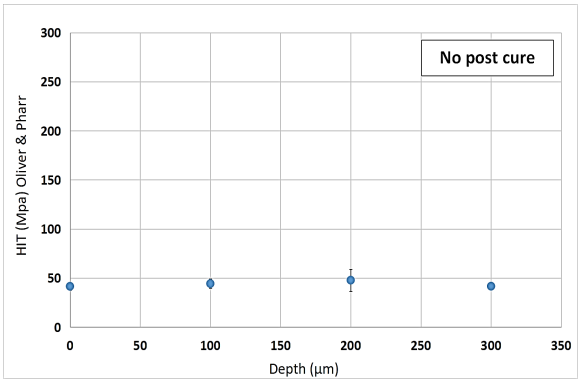

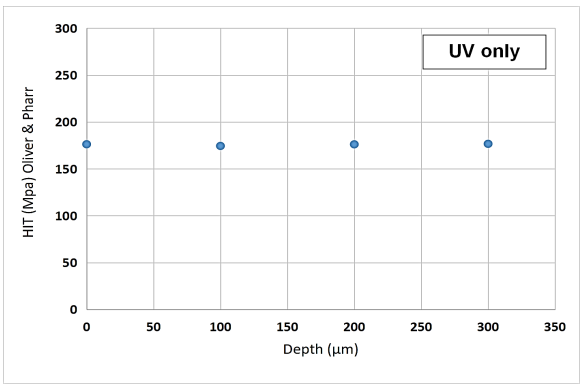

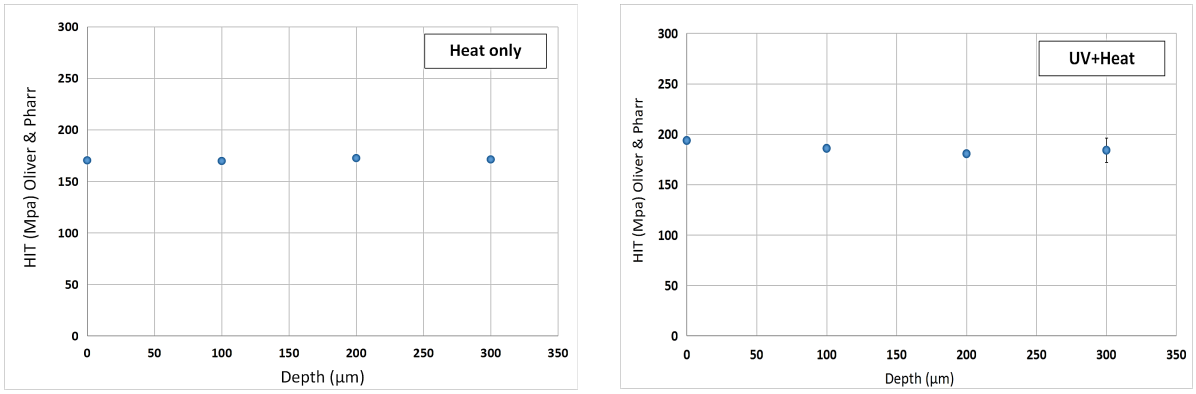

Figure 9: Effect of post-curing process on nano-hardness of System C

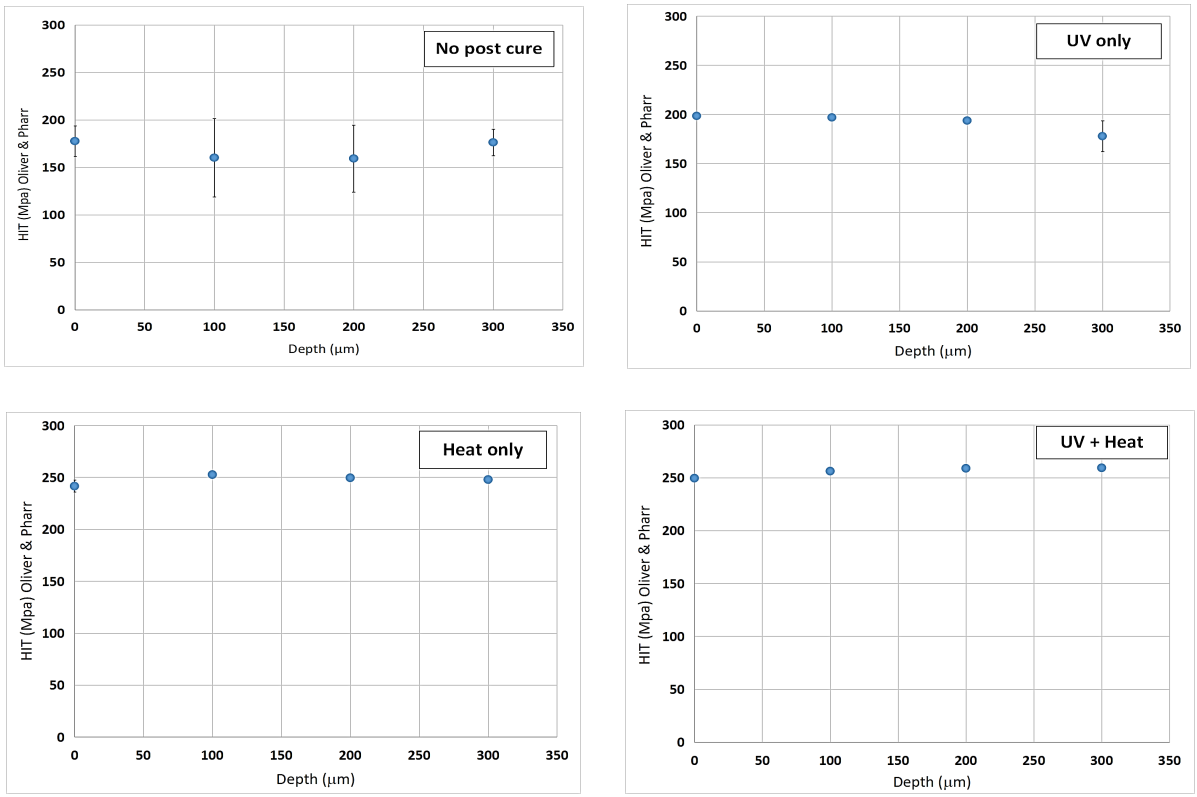

Figure 10: Effect of post-curing process on nano-hardness of System B

3.3. FTIR studies

FTIR spectroscopy was used to track the effect of the post-curing process on the condensation thiol-ene reaction in System B, and free radical polymerization of acrylate double bonds in System C. As displayed in **Figure 11 (a)**, in System B, the absorption peak at 2620 cm^{-1}, which is attributed to S-H stretch, was completely diminished after the post-curing, regardless of the post-curing type. Similarly, the absorptions of C=C stretch at 1637 cm^{-1} and C=C bending at 810 cm^{-1}

were also significantly reduced by post-curing. This shows that polymerization of thiol-ene systems could occur via heating, UV-curing, and EB-curing.

For System C (see **Figure 11 (b)**), UV-curing resulted in a significant reduction in absorptions of C=C stretch at 1637 cm^{-1} and C=C bending at 810 cm^{-1}, while heat-curing resulted in no such significant reduction in absorption of those peaks. Thus, FTIR results are in good alignment with the mechanical property measurements, showing that heat only was not an effective post-cure process for crosslinking.

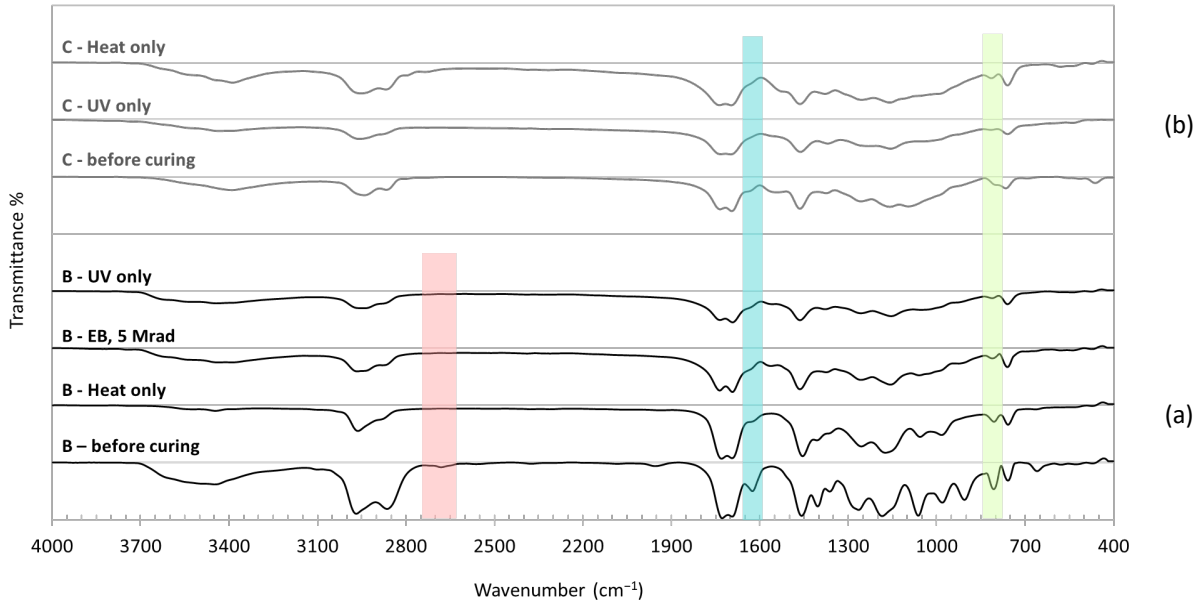

Figure 11: FTIR spectra of (a) System B before and after heat, UV, and EB post-curing processes; and (b) System C before and after heat and UV post-curing processes.

4. Conclusion

The goal of this study was to investigate the effects of various post-curing processes on the mechanical performance of DLP 3D-printed parts for automotive applications, in order to provide a good insight into selecting the proper post-curing method per formulation/application. To this end, three resin systems with two different chemistries were used to print the bars used for Instron testing. The bars where then post-cured using the five following methods: no post-cure, UV-only, heat-only, UV+ heat, and EB-curing. Tensile properties, nano-hardness, and FTIR results demonstrated that thermal curing was not as effective as UV for acrylate-based resins such as System C compared to the two other systems, which could undergo thermal polymerization as well. On the other hand, EB curing, even at very low dosages, was very effective for crosslinking of one of the thio-lene-based resins, to the point of embrittlement for EB dosages above 0.5 Mrad.

Regardless of the type of post-curing, the thio-lene-based resin of System B showed the smallest change in mechanical properties as a result of post-curing. Therefore, post-curing does not seem to be necessary for System B, which could be a benefit in certain applications. Also, System B could be a promising option for the automotive parts that require good retention of tensile properties including %E. Systems A and C did not show a very high %E retention. However, considering their other properties and provided a suitable post-curing process, they might be

suitable options for automotive parts that are not exposed to mechanical forces that could induce dimensional changes.

The current studies indicate that the performance of 3D printed parts can be tailored by a combination of resin chemistry and formulation, print process, and post-cure process. Further and continued investigation is needed to extend the performance to meet stringent automotive requirements.

5. Acknowledgement

The authors would like to thank Sage Schissel, from PCT E-beam and integration company for conducting the EB-curing experiments.

References

(1) Attaran, M. The Rise of 3-D Printing: The Advantages of Additive Manufacturing over Traditional Manufacturing. *Bus. Horiz.* **2017**, *60* (5), 677–688. https://doi.org/10.1016/j.bushor.2017.05.011.

(2) Leal, R.; Barreiros, F. M.; Alves, L.; Romeiro, F.; Vasco, J. C.; Santos, M.; Marto, C. Additive Manufacturing Tooling for the Automotive Industry. *Int. J. Adv. Manuf. Technol.* **2017**, *92* (5–8), 1671–1676. https://doi.org/10.1007/s00170-017-0239-8.

(3) Walker, M.; Humphries, S. 3D Printing: Applications in Evolution and Ecology. *Ecol. Evol.* **2019**, *9* (7), 4289–4301. https://doi.org/10.1002/ece3.5050.

(4) Bagheri, A.; Jin, J. Photopolymerization in 3D Printing. *ACS Appl. Polym. Mater.* **2019**, *1* (4), 593–611. https://doi.org/10.1021/acsapm.8b00165.

(5) Seubert, C. M.; Nichols, M. E. Alternative Curing Methods of UV Curable Automotive Clearcoats. In *Progress in organic coatings.*; 2004; Vol. 49, pp 218–224. https://doi.org/10.1016/j.porgcoat.2003.10.002.

(6) Akdogan, O. K.; Zareanshahraki, F.; Mannari, V. Dual-Cure Polyurethane Coatings from Soybean Oil and Their Film Properties as a Function of Cure Sequence. *J. Lipid Sci. Technol.* **2019**, *50* (4), 112–122.

(7) Zareanshahraki, F.; Asemani, H. R.; Skuza, J.; Mannari, V. Synthesis of Non-Isocyanate Polyurethanes and Their Application in Radiation-Curable Aerospace Coatings. *Prog. Org. Coat.* **2020**, *138* (Journal Article), 105394. https://doi.org/10.1016/j.porgcoat.2019.105394.

(8) Zareanshahraki, F.; Mannari, V. “Green” UV-LED Gel Nail Polishes from Bio-Based Materials. *Int. J. Cosmet. Sci.* **2018**, *40* (6), 555–564. https://doi.org/10.1111/ics.12497.

(9) Bowman, C. N.; Cramer, N. B. New Resin Systems for Dental Restorative Materials. WO2010114760A1, October 7, 2010.

(10) Pappas, S. P. *Radiation Curing: Science and Technology*; Springer Science & Business Media, 2013.

(11) Cramer, N. B.; Reddy, S. K.; O'Brien, A. K.; Bowman, C. N. Thiol−Ene Photopolymerization Mechanism and Rate Limiting Step Changes for Various Vinyl Functional Group Chemistries. *Macromolecules* **2003**, *36* (21), 7964–7969. https://doi.org/10.1021/ma034667s.

(12) Esfandiari, P.; Ligon, S. C.; Lagref, J. J.; Frantz, R.; Cherkaoui, Z.; Liska, R. Efficient Stabilization of Thiol-Ene Formulations in Radical Photopolymerization. *J. Polym. Sci. Part Polym. Chem.* **2013**, *51* (20), 4261–4266. https://doi.org/10.1002/pola.26848.

(13) Seubert, C. M.; Nichols, M. E.; Cooper, V. A.; Gerlock, J. L. The Long-Term Weathering Behavior of UV Curable Clearcoats: I. Bulk Chemical and Physical Analysis. *Polym. Degrad. Stab.* **2003**, *81* (1), 103–115. https://doi.org/10.1016/S0141-3910(03)00079-X.

(14) Zguris, Z. How Mechanical Properties of Stereolithography 3D Prints are Affected by UV Curing https://www.formlabs.com (accessed Oct 16, 2019).

(15) Aznarte, E.; Ayranci, C.; Qureshi, A. Digital Light Processing (DLP) : Anisotropic Tensile Considerations. In *Solid Freeform Fabrication 2017: Proceedings of the 28th Annual International*; 2017; pp 413–425.

(16) Ibrahim, A.; Sa'ude, N.; Ibrahim, M. Optimization of Process Patameter for Digital Light Processing (DLP) 3D Printing. In *Proceedings of Academics World 62nd International Conference, Seoul, South Korea*; Seoul, South Korea, 2017; pp 11–14.

(17) Chockalingam, K.; Jawahar, N.; Chandrasekhar, U. Influence of Layer Thickness on Mechanical Properties in Stereolithography. *Rapid Prototyp. J.* **2006**. https://doi.org/10.1108/13552540610652456.

(18) Bonada, J.; Muguruza, A.; Fernández-Francos, X.; Ramis, X. Influence of Exposure Time on Mechanical Properties and Photocuring Conversion Ratios for Photosensitive Materials Used in Additive Manufacturing. *Procedia Manuf.* **2017**, *13*, 762–769. https://doi.org/10.1016/j.promfg.2017.09.182.

(19) Lee, Y.; Lee, S.; Zhao, X. G.; Lee, D.; Kim, T.; Jung, H.; Kim, N. Impact of UV Curing Process on Mechanical Properties and Dimensional Accuracies of Digital Light Processing 3D Printed Objects. *Smart Struct. Syst.* **2018**, *22* (2), 161–166. https://doi.org/10.12989/sss.2018.22.2.161.

(20) Vitale, A.; Cabral, J. Frontal Conversion and Uniformity in 3D Printing by Photopolymerisation. *MATERIALS* **2016**, *9* (9), 760. https://doi.org/10.3390/ma9090760.

(21) Gundrati, N. B.; Chakraborty, P.; Zhou, C.; Chung, D. D. L. Effects of Printing Conditions on the Molecular Alignment of Three-Dimensionally Printed Polymer. *Compos. Part B Eng.* **2018**, *134*, 164–168. https://doi.org/10.1016/j.compositesb.2017.09.067.

(22) Oliver, W. C.; Pharr, G. M. An Improved Technique for Determining Hardness and Elastic Modulus Using Load and Displacement Sensing Indentation Experiments. *J. Mater. Res.* **1992**, *7* (6), 1564–1583. https://doi.org/10.1557/JMR.1992.1564.

(23) Firdaus, M.; Montero de Espinosa, L.; Meier, M. A. R. Terpene-Based Renewable Monomers and Polymers via Thiol–Ene Additions. *Macromolecules* **2011**, *44* (18), 7253–7262. https://doi.org/10.1021/ma201544e.

(24) Srivastava, S. Co-Polymerization of Acrylates. *Des. Monomers Polym.* **2009**, *12* (1), 1–18. https://doi.org/10.1163/156855508X391103.

(25) Hong, S. Y.; Kim, Y. C.; Kim, H.-I.; Wang, M.; Byun, D.-Y.; Nam, J.-D.; Chou, T.-W.; Ajayan, P. M.; Ci, L.; Suhr, J. Experimental Investigation of Mechanical Properties of UV-Curable 3D Printing Materials. *Polymer* **2018**, *145* (Journal Article), 88–94. https://doi.org/10.1016/j.polymer.2018.04.067.

(26) Johansson, M.; Glauser, T.; Rospo, G.; Hult, A.; Tidigare Institutioner (före 2005); Polymerteknologi; KTH. Radiation Curing of Hyperbranched Polyester Resins. *J. Appl. Polym. Sci.* **2000**, *75* (5), 612–618. https://doi.org/10.1002/(SICI)1097-4628(20000131)75:5<612::AID-APP3>3.0.CO;2-1.